Speckle-field digital holographic microscopy

YongKeun Park[1,2], Wonshik Choi[1,3*], Zahid Yaqoob[1], Ramachandra Dasari[1], Kamran Badizadegan[1,4], and Michael S. Feld[1]

[1]*George R. Harrison Spectroscopy Laboratory, MIT, 77 Massachusetts Avenue, Cambridge, MA 02139, USA*
[2]*Department of Health Science & Technology, Harvard-MIT, 77 Massachusetts Avenue Camridge MA 02139, USA*
[3] *Department of Physics, Korea University, Seoul 136-701, Korea*
[4] *Harvard Medical School and Massachusetts General Hospital, Boston, MA 02114*
**wonshik@mit.edu*

Abstract: The use of coherent light in conventional holographic phase microscopy (HPM) poses three major drawbacks: poor spatial resolution, weak depth sectioning, and fixed pattern noise due to unwanted diffraction. Here, we report a technique which can overcome these drawbacks, but maintains the advantage of phase microscopy - high contrast live cell imaging and 3D imaging. A speckle beam of a complex spatial pattern is used for illumination to reduce fixed pattern noise and to improve optical sectioning capability. By recording of the electric field of speckle, we demonstrate high contrast 3D live cell imaging without the need for axial scanning - neither objective lens nor sample stage. This technique has great potential in studying biological samples with improved sensitivity, resolution and optical sectioning capability.

OCIS codes: (180.0180) Microscopy; (120.0120) Instrumentation, measurement, and metrology; (170.0170) Medical optics and biotechnology.

References and links

1. E. Cuche, F. Bevilacqua, and C. Depeursinge, "Digital holography for quantitative phase-contrast imaging," Opt. Lett. **24**(5), 291–293 (1999).
2. G. Popescu, L. P. Deflores, J. C. Vaughan, K. Badizadegan, H. Iwai, R. R. Dasari, and M. S. Feld, "Fourier phase microscopy for investigation of biological structures and dynamics," Opt. Lett. **29**(21), 2503–2505 (2004).
3. G. Popescu, T. Ikeda, R. R. Dasari, and M. S. Feld, "Diffraction phase microscopy for quantifying cell structure and dynamics," Opt. Lett. **31**(6), 775–777 (2006).
4. Y. K. Park, G. Popescu, K. Badizadegan, R. R. Dasari, and M. S. Feld, "Diffraction phase and fluorescence microscopy," Opt. Express **14**(18), 8263–8268 (2006).
5. C. Mann, L. Yu, C. M. Lo, and M. Kim, "High-resolution quantitative phase-contrast microscopy by digital holography," Opt. Express **13**(22), 8693–8698 (2005).
6. Y.-K. Park, M. Diez-Silva, G. Popescu, G. Lykotrafitis, W. Choi, M. S. Feld, and S. Suresh, "Refractive index maps and membrane dynamics of human red blood cells parasitized by Plasmodium falciparum," Proc. Natl. Acad. Sci. U.S.A. **105**(37), 13730–13735 (2008).
7. G. Popescu, Y.-K. Park, N. Lue, C. Best-Popescu, L. Deflores, R. R. Dasari, M. S. Feld, and K. Badizadegan, "Optical imaging of cell mass and growth dynamics," Am. J. Physiol. Cell Physiol. **295**(2), C538–C544 (2008).
8. G. Popescu, T. Ikeda, C. A. Best, K. Badizadegan, R. R. Dasari, and M. S. Feld, "Erythrocyte structure and dynamics quantified by Hilbert phase microscopy," J. Biomed. Opt. **10**(6), 060503 (2005).
9. Y. K. Park, G. Popescu, K. Badizadegan, R. R. Dasari, and M. S. Feld, "Fresnel particle tracing in three dimensions using diffraction phase microscopy," Opt. Lett. **32**(7), 811–813 (2007).
10. G. Popescu, Y.-K. Park, W. Choi, R. R. Dasari, M. S. Feld, and K. Badizadegan, "Imaging red blood cell dynamics by quantitative phase microscopy," Blood Cells Mol. Dis. **41**(1), 10–16 (2008).
11. B. Rappaz, P. Marquet, E. Cuche, Y. Emery, C. Depeursinge, and P. Magistretti, "Measurement of the integral refractive index and dynamic cell morphometry of living cells with digital holographic microscopy," Opt. Express **13**(23), 9361–9373 (2005).
12. F. Dubois, M. L. Requena, C. Minetti, O. Monnom, and E. Istasse, "Partial spatial coherence effects in digital holographic microscopy with a laser source," Appl. Opt. **43**(5), 1131–1139 (2004).
13. M. G. Somekh, C. W. See, and J. Goh, "Wide field amplitude and phase confocal microscope with speckle illumination," Opt. Commun. **174**(1-4), 75–80 (2000).
14. M. C. Pitter, C. W. See, and M. G. Somekh, "Full-field heterodyne interference microscope with spatially incoherent illumination," Opt. Lett. **29**(11), 1200–1202 (2004).

#110930 - $15.00 USD Received 4 May 2009; revised 25 Jun 2009; accepted 28 Jun 2009; published 6 Jul 2009

15. C. Ventalon, and J. Mertz, "Quasi-confocal fluorescence sectioning with dynamic speckle illumination," Opt. Lett. **30**(24), 3350–3352 (2005).
16. J. Walker, "Non-scanning confocal fluorescence microscopy using speckle illumination," Opt. Commun. **189**(4-6), 221–226 (2001).
17. C. Fang-Yen, S. Oh, Y.-K. Park, W. Choi, S. Song, H. S. Seung, R. R. Dasari, and M. S. Feld, "Imaging voltage-dependent cell motions with heterodyne Mach-Zehnder phase microscopy," Opt. Lett. **32**(11), 1572–1574 (2007).
18. W. Choi, C. Fang-Yen, K. Badizadegan, S. Oh, N. Lue, R. R. Dasari, and M. S. Feld, "Tomographic phase microscopy," Nat. Methods **4**(9), 717–719 (2007).
19. S. Inoue, and K. R. and Spring, *Video Microscopy* (Plenum Press, New York and London, 1997).
20. G. Nomarski, "Microinterféromètre différentiel à ondes polarisées," J. Phys. Radium **16**, 9S–11S (1955).
21. J. Goodman, *Introduction to Fourier optics* (Roberts & Co, 2005).

1. Introduction

Holographic phase microscopy (HPM), an interferometry-based light microscopic technique for sensing complex electric field (E-field) [1–5], has emerged as an important tool for studying structure and dynamics of biological samples [6–11], mainly due to its ability to measure phase changes induced by the sample with nanometer scale accuracy. Conventional HPM typically uses both temporally and spatially coherent light for illumination. Temporal coherence, necessary to accomplish interferometry, causes unwanted diffraction from optical elements and dust particles in the beam path, which results in fixed pattern noise. Spatial coherence is desirable since a well-defined wavefront of illumination beam simplifies extraction of the change in wavefront induced by the sample. The typical method of full-field imaging with a spatially and temporally coherent source is to illuminate a specimen with a collimated plane wave beam. However, employing plane wave illumination makes use of only a very limited aperture in a condenser lens. This leads to poor spatial resolution compared with diffraction-limited resolution of conventional bright field microscopy.

Conventional bright field microscopy uses incoherent sources such as a thermal light, which allows full-field illumination on the sample and, at the same time, enables utilization of full aperture of the condenser lens to guarantee diffraction-limited resolution. To take the advantages of incoherent illumination in HPM, a speckle beam can be used which is generated by illuminating temporally coherent source through a diffuser such as a ground glass and a holographic diffuser. The speckle beam enables to utilize full condenser aperture as well as to allow full-field illumination. However, it exhibits large intensity variations across the field of view. In case of thermal source, temporal incoherence with longer data acquisition time than the coherence time eliminates non-uniform speckle pattern by random temporal averaging, leading to a clean imaging. We note that there have been studies in which time varying speckles were used for HPM to eliminate non-uniform intensity distribution [12–14]. A rotating ground glass or a moving diffuser was used to change speckle patterns in time. As a result, the transmitted light becomes incoherent in time and space, which lead to improvement in image performance: reducing the effect of unwanted diffractions, improving spatial resolution and providing confocal-equivalent sectioning. These studies have imaged time-averaged multiple speckles, not the recording of the individual speckle field, which is beneficial in data acquisition time since only single E-field recording is necessary. However, to acquire 3D imaging capability, complicated numerical propagation problem has to be solved for the time-averaged speckle field, which was previously demonstrated in paraxial condition with low numerical aperture [12]. The speckle beam was also used in wide-field fluorescence imaging [15,16] to improve resolution and sectioning ability.

In this report, we present a novel imaging technique, called speckle-field digital holographic microscopy (SDHM), which utilizes the speckle field for illumination. By synthesizing E-field images of speckle, we significantly improve image quality and spatial resolution compared with conventional HPM. Recording of individual speckle pattern makes it straightforward to use angular spectrum method, valid for high numerical aperture condition, to solve numerical propagation. As a result, 3D images are obtained without

#110930 - $15.00 USD Received 4 May 2009; revised 25 Jun 2009; accepted 28 Jun 2009; published 6 Jul 2009

scanning either objective lens or sample stage. The technique is applied to imaging biological cells to visualize intracellular features.

2. Principle of speckle field holographic microscopy

We first present a brief description of extracting a sample-induced phase delay with speckle illumination (Fig. 1). We generated a speckle field by illuminating a holographic diffuser (NT54-494, Edmund Optics Inc.) with a He-Ne laser (Coherent Inc.). The speckle field traveled through a microscope and was imaged on a detector. The hologram of the speckle field was generated by imposing a plane-wave reference beam on the detector. (Fig. 1a). Using a heterodyne Mach-Zehnder interferometer [17], a complex E-field of the speckle was retrieved, as shown in Figs. 1(b-c). Then, a sample (polystyrene bead of 10 μm diameter, Thermo Fisher Scientific Inc.) submerged in immersion oil, was inserted on the sample stage with the same speckle field illumination. Introducing the sample modified the original speckle pattern. Next, the E-field of the modified speckle was recorded in the same way as the recording of the original speckle pattern (Figs. 1d-e). The sample is almost invisible in these images since its image is overlapped with the complex pattern of the speckle field. We note that the speckle is stationary, as the coherence length of the laser is much larger than the scattering length of the diffuser. Therefore, the background speckle field can be removed and the sample-induced complex field image can be retrieved from the speckle field (Fig. 1b-c) by dividing it by the field without the sample (Fig. 1d-e). As a result, the sample becomes clearly visible, as shown in Figs. 1f-g.

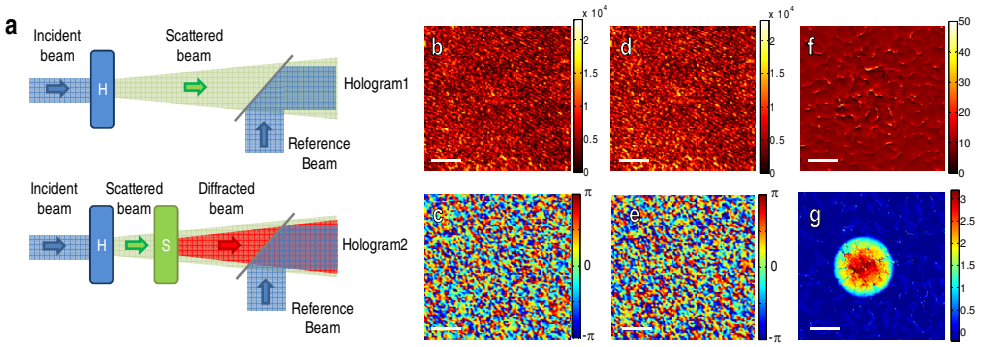

Fig. 1. (a) Principle of speckle field holographic microscopy. A holographic diffuser (H) is illuminated with a laser beam. The complex E-field of the scattered beam is measured from the interference image (hologram 1) after interference with a reference beam. After introducing a sample (S), another interference image is measured (hologram 2). (b-c) amplitude (b) and phase (c) of the E-field without the sample, (d-e) amplitude (d) and phase (e) with the sample. (f-g) Amplitude (f) and phase (g) are images of the sample, a 10 μm polystyrene bead. Scale bar, 5 μm. Colorbars indicate arbitrary units for the amplitude and radians for the phase, respectively.

Accurate E-field recording of speckle enabled us to account for the random distribution of speckle and thus to retrieve sample image. There exist, however, singular points in the resulting amplitude and phase maps (Fig. 1f-g). This is because the phase is ill-defined at the dark spots of the measured speckle pattern, which result from the destructive interference of a set of plane waves consisting of the speckle. In order to eliminate these singular points, previous study [13] and conventional bright field imaging have utilized a temporally incoherent source together with time averaging. In our approach, we performed multiple measurements with different speckle patterns and synthesized them afterwards. For the systematic control of speckle patterns, we set up an experiment as shown in Fig. 2(a) [18]. Galvanometer mirrors in the sample beam path controlled the incident angle of a laser beam to the diffuser and generated angle-dependent speckle fields. Two sets of angle-dependent

#110930 - $15.00 USD Received 4 May 2009; revised 25 Jun 2009; accepted 28 Jun 2009; published 6 Jul 2009

speckle images were recorded, one with the sample and the other without it. It took about 1.4 seconds to record 100 speckle fields for the results shown in Fig. 2. Then, a set of net angle-dependent E-field images were obtained after dividing one set with the sample by the other without it. Since the distribution of dark spots and hence the singular points varies with the change speckle patterns, we removed the singular points by averaging multiple angle-dependent E-field images. The processed images are shown in Figs. 2(b-e), where N represents the number of speckle images used for averaging. It is shown that the number of singular points was significantly decreased and the noise in the synthesized image was greatly attenuated as we increase the number of speckle images. To quantify the improvement of the phase detection sensitivity, we plot the standard deviation of phase averaged for an area of 4 × 4 μm^2 located outside of the sample. As shown in Fig. 2(f), the standard deviation of phase decreases from 9 nm to 1 nm as we increased the number of speckle images from 1 to 100.

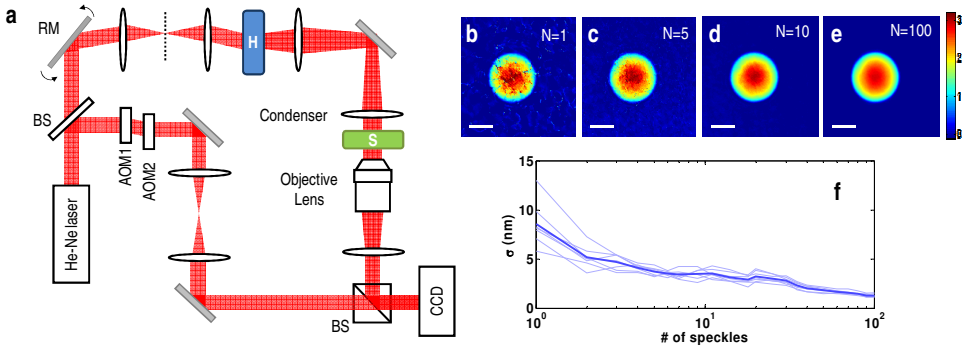

Fig. 2. (a) Experimental setup. BS: beam splitter, GM: galvanometer mirrors, H: a holographic diffuser, S: sample, Condenser: Nikon 1.4NA, Camera: (Fastcam 1024 PCI, Photron), AOM1,2: acousto-optic modulators for temporal modulation of interference by shifting the frequency of the reference beam. (b-e) Averaged phase images where N is the number of speckle fields used for averaging. Scale bar indicates 5 μm and color bar indicates radian. (f) Standard deviation of phase noise as a function of the number of speckle fields used for averaging. Thin lines indicate the averaged phase for an area of 4 × 4 μm^2 located outside of the sample. Thick line shows the averaged phase for 6 different areas.

3. Imaging capabilities of speckle field holographic microscopy

We compared the image quality of SDHM with a conventional HPM. HPM images were taken with a plane-wave illumination, which was achieved by simply removing a holographic diffuser in the beam path. A 10 μm polystyrene bead was used as a phase object and a USAF 1951 resolution target (Edmund Optics Inc.) as an absorptive object. Figures 3(a-c) are HPM images of the 10 μm bead and USAF resolution target, and SDHM images of the same samples are shown in Figs. 3(d-f). Inherent fixed pattern noise, induced by the diffraction from scatterers in the beam path, is visible in the HPM images, which degrades the overall image quality. In contrast, the fixed pattern noise was attenuated in SDHM due to the spatially incoherent illumination. Thus, SDHM successfully took advantage of incoherent illumination into coherent field measurement. Speckle illumination not only reduces diffraction noise but also enhances the resolution in comparison with conventional HPM. Speckle is composed of multiple angular plane waves. The larger the angular range is, the speckle pattern is finer and the spatial resolution becomes better. The angular range for the illumination can be quantified by the illumination numerical aperture (NA), $NA_I = n \cdot sin\theta_{max}$, where θ_{max} is the maximum angle of a plane wave constituting the speckle with respect to the optic axis. NA_I of conventional HPM is almost close to zero. In SDHM, we overfill the back focal plane of illumination condenser by use of holographic diffuser to maximize the use of condenser NA (Nikon, 1.4 NA). For non-luminous specimen such as biological cells and polystyrene beads,

#110930 - $15.00 USD Received 4 May 2009; revised 25 Jun 2009; accepted 28 Jun 2009; published 6 Jul 2009

the diffraction-limited resolution is determined by both the objective NA and illumination NA, and is given by [19]:

$$d = 1.22\lambda / (NA_O + NA_I), \quad (1)$$

where λ is the wavelength of light source, NA_O is the objective NA and NA_I the illumination NA. In our experiment, we used the same numerical aperture for both NA_O and NA_I. Therefore, we expect the spatial resolving power of SDHM twice better than that of HPM.

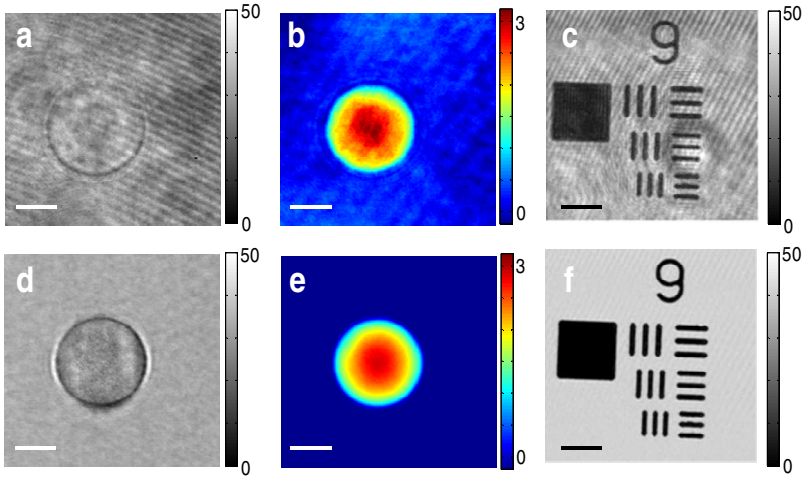

Fig. 3. (a) Amplitude and (b) phase images of the E-field measured for a 10 μm polystyrene bead with a conventional HPM. (d) Amplitude and (e) phase images of the same sample measure by SDHM. (c, f), Amplitude images of USAF resolution (group 9) target measured by conventional HPM and SDHM, respectively. Scale bar indicates 5 μm, and colorbars indicate arbitrary unit for amplitude images and radians for the phase images, respectively. For SDHM, 100 raw images are processed to reduce singularity points.

To verify the enhancement in image resolution, we measured a cluster of polystyrene beads of 200 nm diameter each (Thermo Fisher Scientific Inc.), where the feature size is smaller than the diffraction-limited resolution. An Ar^+ laser (λ = 488 nm, Coherent Inc.) is used for this experiment. Note that the effective NA of the objective and the illumination was 1, since we placed the beads in air. The theoretical spatial resolution is 595 nm for HPM and 298 nm for SDHM. Phase images taken by HPM are shown in Figs. 4(a-d), whereas Figs. 4(e-f) present phase images taken by SDHM for the same samples. Notice that adjacent beads could not be resolved in phase maps acquired by HPM (Figs. 4a-c). In contrast, neighboring beads were clearly resolved in SDHM images (Figs. 4e-g) as indicated by white arrows. To quantify the enhancement in spatial resolution, we retrieved the lateral point spread functions of HPM and SDHM (Fig. 4j). The point spread function of the system was calculated by deconvolution between the measured phase image of a 200 nm polystyrene bead and the ideal phase delay map of the beads. The widths of the point spread functions are reduced after using speckle field, which demonstrates clear advantages of SDHM for improvement in lateral resolution. The full width half maximum of the point spread function were 516 nm for HPM and 305 nm for SDHM, which are very close to the theoretical expectations. It is noteworthy that there exists a pronounced oscillatory tail only for HPM, which is the consequence of coherent illumination. We also assessed the axial resolution. 3D images of the same single bead were obtained by the numerical propagation of the coherent and speckle fields, as described in the next section. Then, axial point spread functions were calculated by deconvolving the axial profiles. The axial point spread functions for both HPM and SDHM

#110930 - $15.00 USD Received 4 May 2009; revised 25 Jun 2009; accepted 28 Jun 2009; published 6 Jul 2009

are shown in Fig. 4(j), which illustrates that the axial resolution of SDHM (1.51 μm) is 1.63 times better than that of HPM (2.46 μm).

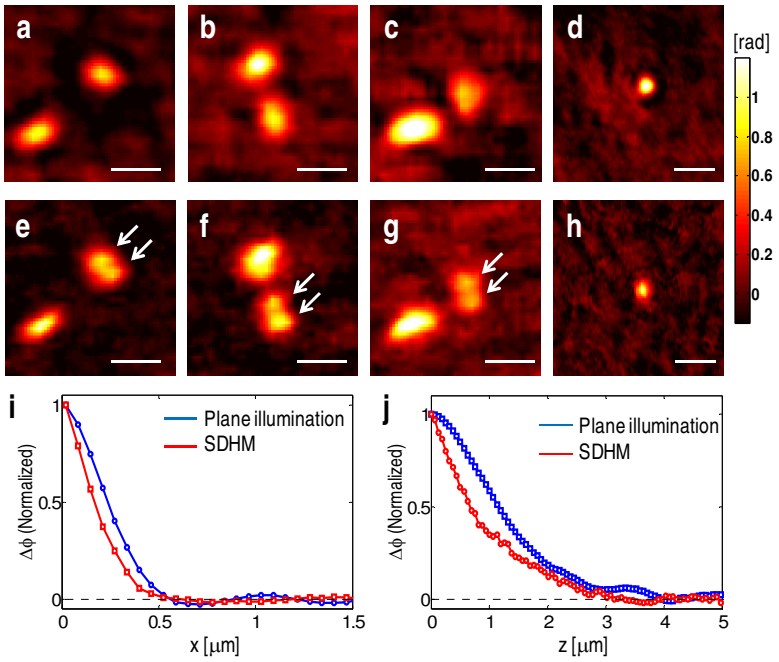

Fig. 4. Speckle illumination increases lateral and axial resolving power. (a-d) Phase maps of polystyrene beads (200nm diameter) measured with a conventional HPM. (e-h) Phase maps measured with a speckle illumination of the same samples in (a-d). Scale bar indicates 500 nm. (i) Lateral point spread functions of a conventional HPM (blue line) and a speckle illumination (red line). (j) Axial point spread functions of a conventional HPM (blue line) and a speckle illumination (red line). For SDHM, 50 raw E-field images are processed to reduce singularity points.

4. 3D live cell imaging

We applied SDHM to high resolution imaging of biological samples. HeLa cells submerged in phosphate buffered saline solution (PBS) were placed between two cover-slips and imaged using both HPM and SDHM (Fig. 5). As seen in Figs. 5(a,c), sub-cellular particles exhibited diffraction patterns in HPM, but were clearly resolved in SDHM (Figs. 5b,d). With this improved complex E-field image technique, we numerically emulated differential interference contrast (DIC) microscopy [20]. In DIC microscopy, a complex E-field containing sample image is physically shifted by an amount close to the diffraction-limited resolution and is recombined with original E-field to form a high contrast interference image. In our study, we numerically shifted the measured complex E-field image, which provides us with the flexibility in both shearing direction as well as bias retardation. The interference intensity is given by $I_{DIC} = \left| f(x,y) + f(x+\Delta x, y+\Delta y) e^{j\Delta\varphi} \right|^2$, where $f(x,y)$, Δx, Δy, and $\Delta\phi$ are a complex E-field image, x-directional shifting, y-directional shifting and bias retardation, respectively. Results from numerical DIC images based on SDHM are shown in Fig. 5(g). The image contrast is significantly enhanced compared with either amplitude (Fig. 5b) or phase image (Fig. 5d). The small sub-cellular organelles such as nucleus and micro vesicles are clearly visible. Note that the same numerical DIC operation is also applicable to conventional HPM, as shown in Fig. 5(e). However the enhanced contrast of fixed pattern noise has dominated the contrast of the sample's sub-cellular features.

#110930 - $15.00 USD Received 4 May 2009; revised 25 Jun 2009; accepted 28 Jun 2009; published 6 Jul 2009

In conventional DIC and previous speckle-illumination based interferometry [13,14], either objective lens or sample stage has to be scanned to obtain 3D imaging. Since a complex E-field of individual speckle image was recorded in our study, we can numerically propagate the individual E-field in axial direction using the angular spectrum method [21]. Thus, 3D images of a cell can be obtained without axial scanning. In order to obtain DIC images at different sections, we first numerically propagated all the speckle fields taken with and without the sample at the same distance. Two sets of propagated E-field images were then processed to form a synthesized E-field image and a corresponding DIC image. Following is the brief description of the numerical far field propagation method. The complex E-field, $f(x,y;z=0)=A(x,y)e^{j\varphi(x,y)}$ where $A(x,y)$ and $\varphi(x,y)$ are amplitude and phase, respectively, can be decomposed into a superposition of plane waves; $f(x,y;0)=\iint F(\nu_x,\nu_y)e^{-2\pi j(\nu_x x+\nu_y y)}d\nu_x d\nu_y$, where ν_x,ν_y are the spatial frequencies along the x- and y-axis. For field propagation, each plane wave is propagated and recombined as follows, $f(x,y)=\iint F(\nu_x,\nu_y)e^{-2\pi j(\nu_x x+\nu_y y)}e^{-2\pi j\nu_z z}d\nu_x d\nu_y$, where $\nu_z=\sqrt{\nu^2-\nu_x^2-\nu_y^2}$ is z-directional spatial frequency.

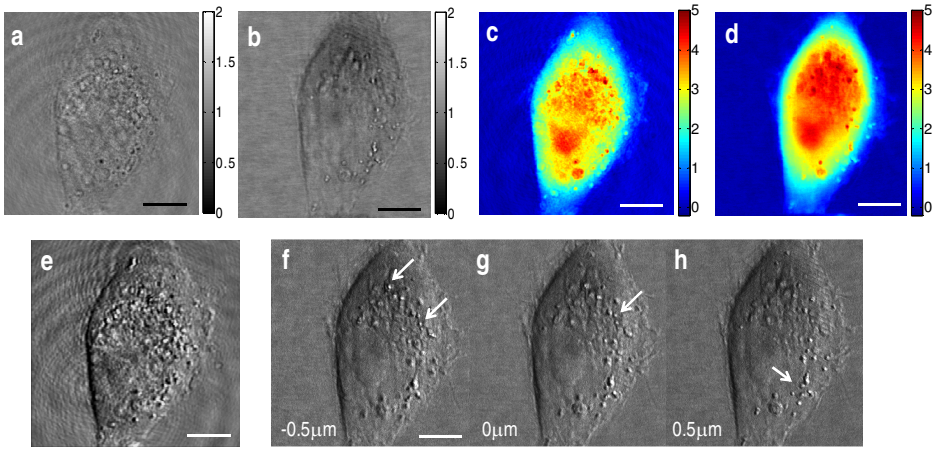

Fig. 5. 3D live cell imaging using SDHM. (a-b) Amplitude maps of a HeLa cell measured with (a) HPM and (b) SDHM, respectively. Color bar indicates arbitrary unit of amplitude. (c-d) Quantitative phase maps of the same cell imaged using HPM and SDHM, respectively. Color bar indicates phase in radian. (e) Emulated differential interference contract (DIC) images of the same cell taken by HPM. (f-h) Emulated DIC images by SDHM; (f) and (h) show numerically propagated DIC images 0.5 μm below and above form the original focus plane (g), respectively. Arrows indicate sub-cellular particles or vesicles focused on the specific focal planes. Scale bar indicates 5 μm. For SDHM, 50 raw E-field images are processed to reduce singularity points.

Figure 5(f) and Fig. 5(h) are emulated DIC images propagated by 0.5 μm toward and away from the objective lens, respectively. As can be seen, intracellular particles were well in focus at the specific focal planes (indicated as arrows) and they became blurred out and disappeared when the images were propagated. This demonstrates the depth discrimination ability of the imaging process, and therefore the 3D imaging capability of SDHM. As a result, we could observe details of structures located at various depths without need for physical z-scanning.

5. Summary and conclusion

We have demonstrated that the speckle-field digital holographic microcopy (SDHM) provides 3D images of complex E-field with high spatial resolution, free of diffraction noise and improved depth sectioning. SDHM combines the advantages of incoherent imaging in

#110930 - $15.00 USD Received 4 May 2009; revised 25 Jun 2009; accepted 28 Jun 2009; published 6 Jul 2009

resolution and image cleanness, with the merit of coherent imaging in complex E-field recording and 3D imaging. The SDHM can also be applicable to the 3D dynamic imaging. Single E-field imaging takes 800 μs, and approximately 50 raw E-field images are required to reconstruct a clean SDPM image. With proper optimization of galvanometer scanning scheme, we will be able to take 3D dynamic SDPM images at 25 fps. As we demonstrated in imaging biological samples, this technique will find immediate applications in studying the 3D dynamics of small sub-cellular structures. SDHM may also be applicable to other imaging fields, such as X-ray and ultra sound imaging.

Acknowledgements

This work was funded by the National Center for Research Resources of the National Institutes of Health (P41-RR02594), the National Science Foundation (DBI-0754339) and Hamamatsu Corporation. Y.-K. Park was supported by Samsung Scholarship and Whitaker Health Science Fellowship.

#110930 - $15.00 USD Received 4 May 2009; revised 25 Jun 2009; accepted 28 Jun 2009; published 6 Jul 2009